

## GALACTIC EMISSION AT 19 GHz

ANGÉLICA DE OLIVEIRA-COSTA,<sup>1,2</sup> MAX TEGMARK,<sup>2,3</sup> LYMAN A. PAGE,<sup>1</sup> AND STEPHEN P. BOUGHN<sup>4</sup>

*Received 1998 August 4; accepted 1998 October 8; published 1998 October 29*

### ABSTRACT

We cross-correlate a 19 GHz full sky cosmic microwave background survey with other maps to quantify the foreground contribution. Correlations are detected with the DIRBE 240, 140, and 100  $\mu\text{m}$  maps at high latitudes ( $|b| > 30^\circ$ ), and marginal correlations are detected with the Haslam 408 MHz and the Reich & Reich 1420 MHz synchrotron maps. The former agree well with extrapolations from higher frequencies probed by the *COBE* Differential Microwave Radiometer and Saskatoon experiments and are consistent with both free-free and rotating dust grain emission.

*Subject headings:* cosmic microwave background — methods: data analysis

### 1. INTRODUCTION

One of the major challenges in any cosmic microwave background (CMB) anisotropy analysis is to determine the fraction of the observed signal due to diffuse Galactic emission. Three components of Galactic emission have been firmly identified: synchrotron and free-free radiation, which are important mainly at frequencies below 60 GHz, and thermal emission from dust particles, which is important mainly at frequencies above 60 GHz (see, e.g., Weiss 1980; Bennett et al. 1992; Brandt et al. 1994; Tegmark & Efstathiou 1996). In principle, these three components can be discriminated by their frequency dependence and morphology. In practice, however, there is no emission component for which both the frequency dependence and the spatial template are currently well known (see, e.g., Kogut et al. 1996a, and references therein).

The cross-correlation technique allows one to estimate the rms level of Galactic emission present in a CMB map. For instance, an analysis of high-latitude Galactic emission in the *COBE* Differential Microwave Radiometer (DMR) map gave rms estimates of  $(3.4 \pm 3.7) \mu\text{K}$  for synchrotron and  $(2.7 \pm 1.3) \mu\text{K}$  for dust emission at 53 GHz on a  $7^\circ$  scale (Kogut et al. 1996b, hereafter K96b). A third component, correlated with the DIRBE maps but decreasing with frequency, was detected at the level of  $(7.1 \pm 1.7) \mu\text{K}$  and was tentatively identified as free-free emission (K96b). Although this component was also detected in the Saskatoon maps (de Oliveira-Costa et al. 1997) on a  $1^\circ$  scale, at a level  $(17.5 \pm 9.5) \mu\text{K}$  at 40 GHz, it is still not clear if it is due to free-free emission. An analysis of Owens Valley Radio Observatory data at 14.5 GHz showed such a component at the level of 203  $\mu\text{K}$  in a small sky region on scales of  $7'–22'$  (Leitch et al. 1997, hereafter L97), but this level is substantially higher than free-free emission estimates based on H $\alpha$  images (Gaustad et al. 1996; Simonetti et al. 1996). Suggested explanations include the presence of high-temperature gas (L97) and rotating dust grains (Draine & Lazarian 1998), but more observational data is needed to settle this issue. The purpose of this Letter is to evaluate the Galactic contribution in the 19 GHz full sky map (see Fig. 1) by cross-correlating it with the DIRBE dust maps and with the Haslam and Reich & Reich synchrotron maps.

### 2. METHOD

The 19 GHz map consists of  $N = 24,576$  pixels with sky temperatures  $y_i$  and noise  $n_i$ . We assume that this map is a superposition of CMB fluctuations and a Galactic component whose angular distribution is traced in part by an external data set. Representing these contributions by  $N$ -dimensional vectors,

$$\mathbf{y} = \mathbf{n} + \mathbf{x}_{\text{CMB}} + \alpha \mathbf{x}_{\text{Gal}} + \mathbf{y}_{\text{Gal}}, \quad (1)$$

where  $x_{\text{CMB}}^i$  is the contribution of the fluctuating component of the CMB,  $x_{\text{Gal}}^i$  is the brightness fluctuations of the Galactic template map (not necessarily in temperature units),  $\alpha$  is the coefficient that converts units of the Galactic template into antenna temperature, and  $y_{\text{Gal}}^i$  represents any residual Galactic contribution which is uncorrelated with  $x_{\text{Gal}}^i$ . We consider  $\mathbf{n}$  and  $\mathbf{x}_{\text{CMB}}$  to be random variables with zero mean, i.e.,  $\langle \mathbf{x}_{\text{CMB}} \rangle = \langle \mathbf{n} \rangle = 0$ , and  $\mathbf{x}_{\text{Gal}}$  and  $\mathbf{y}_{\text{Gal}}$  to be constant vectors. Thus, the data covariance matrix is given by

$$\mathbf{C} \equiv \langle \mathbf{y} \mathbf{y}^T \rangle - \langle \mathbf{y} \rangle \langle \mathbf{y}^T \rangle = \langle \mathbf{x}_{\text{CMB}} \mathbf{x}_{\text{CMB}}^T \rangle + \langle \mathbf{n} \mathbf{n}^T \rangle, \quad (2)$$

where  $\langle \mathbf{x}_{\text{CMB}} \mathbf{x}_{\text{CMB}}^T \rangle$  is the covariance matrix of the CMB and  $\langle \mathbf{n} \mathbf{n}^T \rangle$  is the noise covariance matrix. The noise in the 19 GHz map is approximately uncorrelated and has a known rms amplitude of  $\sigma_i \sim 2$  mK. Therefore, the covariance matrix of this map is

$$C_{ij} \approx \langle n_i n_j \rangle \approx \sigma_i^2 \delta_{ij}. \quad (3)$$

Minimizing  $\chi^2 \equiv (\mathbf{y} - \alpha \mathbf{x}_{\text{Gal}})^T \mathbf{C}^{-1} (\mathbf{y} - \alpha \mathbf{x}_{\text{Gal}})$  yields the minimum-variance estimate of  $\alpha$ , i.e.,

$$\hat{\alpha} = \frac{\mathbf{x}_{\text{Gal}}^T \mathbf{C}^{-1} \mathbf{y}}{\mathbf{x}_{\text{Gal}}^T \mathbf{C}^{-1} \mathbf{x}_{\text{Gal}}} \quad (4)$$

with variance

$$\Delta \hat{\alpha}^2 = \frac{1}{(\mathbf{x}_{\text{Gal}}^T \mathbf{C}^{-1} \mathbf{x}_{\text{Gal}})}. \quad (5)$$

<sup>1</sup> Princeton University, Department of Physics, Princeton, NJ 08544; angelica@ias.edu.

<sup>2</sup> Institute for Advanced Study, Olden Lane, Princeton, NJ 08540.

<sup>3</sup> Hubble Fellow.

<sup>4</sup> Haverford College, Department of Astronomy, Haverford, PA 19041.

Note that unlike the case in de Oliveira-Costa et al. (1997), there is little contribution from chance alignments between the CMB and the various template maps, since the CMB contribution to  $\mathbf{C}$  is negligible. If the noise is correlated or the an-

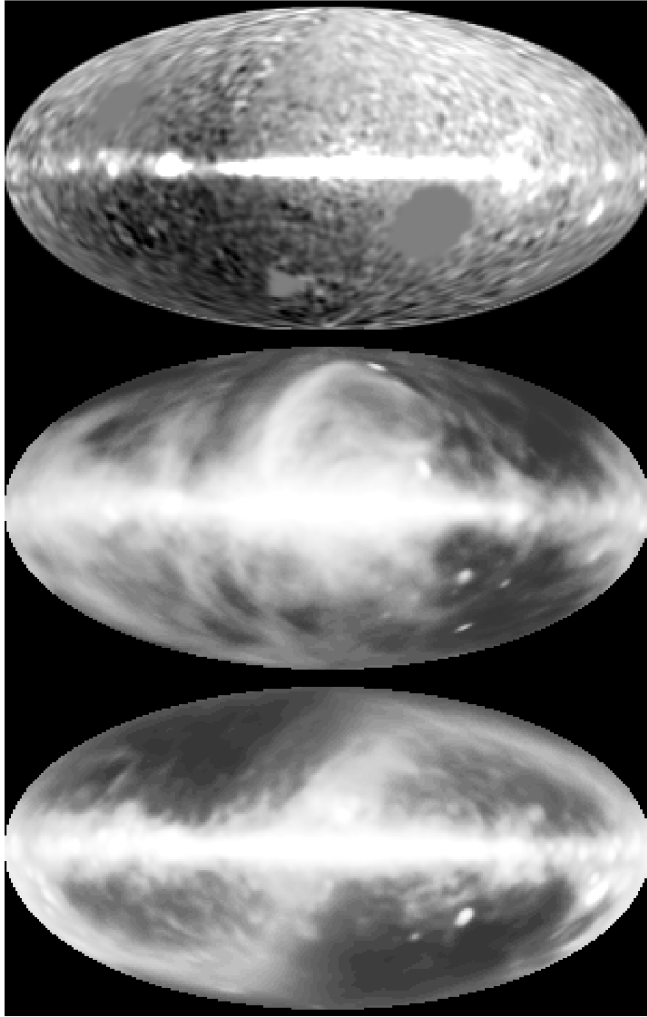


FIG. 1.—The 19 GHz survey (*top*), 408 MHz Haslam synchrotron template (*middle*), and DIRBE 100  $\mu\text{m}$  dust template (*bottom*).

isotropy signal is significant, then our  $\mathbf{C}$  used above will differ from the true covariance matrix, denoted  $\mathbf{C}'$ . Although equation (4) still provides a reasonable and unbiased estimate of  $\alpha$ ,<sup>5</sup> its variance will be larger than implied by equation (5), given by

$$\Delta\hat{\alpha}^2 = \frac{(\mathbf{x}_{\text{Gal}}^T \mathbf{C}^{-1} \mathbf{C}' \mathbf{C}^{-1} \mathbf{x}_{\text{Gal}})}{(\mathbf{x}_{\text{Gal}}^T \mathbf{C}^{-1} \mathbf{x}_{\text{Gal}})^2}. \quad (6)$$

In the next section, an estimate of  $\mathbf{C}'$  is made from the data and the corresponding variance of  $\hat{\alpha}$  is evaluated.

### 3. DATA ANALYSIS AND RESULTS

The 19 GHz map has an angular resolution of  $3^\circ$  FWHM and is stored in  $1:3 \times 1:3$  pixels (Cottingham 1987; Boughn et al. 1992). The template maps are convolved with a  $3^\circ$  Gaussian beam, and regions within  $20^\circ$  and  $30^\circ$  of the Galactic plane are excluded. To avoid contamination by zodiacal dust emission, data within  $10^\circ$  of the ecliptic plane are also excluded from the analysis, although the results are found to be independent of this cut. Off the Galactic plane, the 19 GHz map

<sup>5</sup> Note that the diagonal approximation of eq. (3) reduces eq. (4) to a simple noise-weighted least-squares fit.

TABLE 1  
CORRELATIONS WITH THE 19 GHz MAP

Template	$\hat{\alpha}^a$	$\Delta\hat{\alpha}$	$\Delta\hat{\alpha}_M$	$\Delta\hat{\alpha}_T$	$\delta T^b$ ( $\mu\text{K}$ )
$ b  > 20^\circ$					
100 $\mu\text{m}$ .....	38.5	3.3	5.8	8.3	$138.6 \pm 29.9$
140 $\mu\text{m}$ .....	29.8	2.5	4.0	6.3	$146.0 \pm 30.9$
240 $\mu\text{m}$ .....	46.2	3.9	6.0	10.0	$143.2 \pm 31.0$
408 MHz .....	13.4	3.1	3.4	4.4	$52.3 \pm 17.2$
1420 MHz .....	0.9	0.1	0.2	0.3	$86.5 \pm 28.8$
$ b  > 30^\circ$					
100 $\mu\text{m}$ .....	47.1	9.0	16.2	17.3	$65.9 \pm 24.2$
140 $\mu\text{m}$ .....	31.6	6.3	10.2	10.3	$66.4 \pm 21.6$
240 $\mu\text{m}$ .....	38.9	8.4	12.8	12.9	$66.1 \pm 21.9$
408 MHz .....	7.6	3.7	4.7	6.2	$25.1 \pm 20.5$
1420 MHz .....	0.4	0.2	0.2	0.3	$29.8 \pm 22.3$

<sup>a</sup>  $\hat{\alpha}$  has units  $\mu\text{K} (\text{MJy sr}^{-1})^{-1}$  for the DIRBE templates,  $\mu\text{K/K}$  for the 408 MHz template, and  $\mu\text{K/mK}$  for the 1420 MHz template.

<sup>b</sup>  $\delta T \equiv (\hat{\alpha} \pm \Delta\hat{\alpha}_T)\sigma_{\text{Gal}}$ .

is dominated by the CMB dipole ( $\ell = 1$ ). On the other hand, because of its planar structure, emission associated with the Galaxy has a strong quadrupole ( $\ell = 2$ ) component. Therefore, the monopole, dipole, and quadrupole moments are removed from both the 19 GHz and template maps. As a consequence, the computed  $\hat{\alpha}$  depends only on correlated structure in the maps on angular scales  $\lesssim 90^\circ$ .

#### 3.1. Correlations and Their Error Bars

The 19 GHz map was cross-correlated with five different templates: two for synchrotron emission—the 408 MHz (Haslam et al. 1981) and 1420 MHz (Reich & Reich 1988) surveys—and three to study dust and free-free emission—the 100, 140, and 240  $\mu\text{m}$  DIRBE sky maps (Boggess et al. 1992). Table 1 lists the coefficients  $\hat{\alpha}$  derived from equation (4) with errors computed from equation (5). All three DIRBE templates show significant correlations with the 19 GHz map, while the two synchrotron templates are found to be only marginally correlated.

Also listed in Table 1 are the implied fluctuations in antenna temperature in the 19 GHz map, i.e.,  $\delta T = \hat{\alpha}\sigma_{\text{Gal}}$ , where  $\sigma_{\text{Gal}}$  is the rms of the template map. If a template map includes a distinct component that is uncorrelated with the 19 GHz map, then  $\delta T$  is underestimated by a factor  $\sigma'_{\text{Gal}}/\sigma_{\text{Gal}}$ , where  $\sigma'_{\text{Gal}}$  is the rms of the correlated component of the template map. For this reason, the  $\delta T$ 's in Table 1 should be considered lower limits.

As mentioned above, the errors listed in Table 1 were computed from equation (5) and are therefore lower limits to the error. We now describe a series of tests, performed to estimate the uncertainty in  $\hat{\alpha}$  due to correlated noise and other systematics.

##### 3.1.1. The Noise Correlation Function

If the true noise correlation matrix is isotropic,  $C'_{ij} = \langle n_i n_j \rangle = R(\theta_{ij})\sigma_i\sigma_j$ , where  $\theta_{ij}$  is the angle between pixels  $i$  and  $j$ , then we can estimate the noise correlation function  $R(\theta)$  of the 19 GHz data (after removing the monopole, dipole, and quadrupole) by  $R(\theta) = N_\theta^{-1} \sum_{ij} y_i y_j / \sigma_i \sigma_j$ , where  $y_i$  is the antenna temperature of the  $i$ th pixel and the sum is over all  $N_\theta$  pairs of pixels separated by  $\theta$ . Substituting these relations into equation (6) gives estimates of  $\Delta\hat{\alpha}$  that are from 6% to 17% larger than those in Table 1.

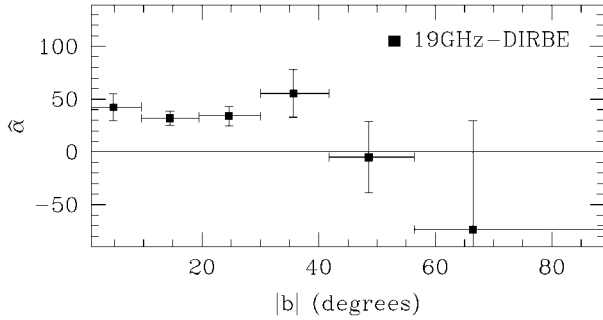


FIG. 2.—Dependence of  $\hat{\alpha}$  on Galactic latitude  $|b|$  for the 100  $\mu\text{m}$  map. The error bars are given by  $\Delta\hat{\alpha}_T$ .

### 3.1.2. Monte Carlo Simulations

As another test of the robustness of the estimates of  $\hat{\alpha}$ , we employed Monte Carlo simulations in which the template maps are sliced into 18 regions of equal area, each corresponding to a range of Galactic latitude  $|b|$ . Inside each of these regions the pixels are rearranged in random order, so that the latitude dependence is preserved but the longitudinal correlations are destroyed. Repeating this procedure 1000 times yields distributions of  $\hat{\alpha}$ 's consistent with zero mean and with standard deviations  $\Delta\hat{\alpha}_M \sim 1.6$  times larger than the formal errors  $\Delta\hat{\alpha}$  (see Table 1).

### 3.1.3. Sky Rotations

Because of the approximate axial symmetry of the Galaxy, it is natural to ask if the correlations are simply due to overall large-scale Galactic structure common to all emission components. To test this hypothesis, we repeated the analysis with  $2 \times 2 \times 36 = 144$  transformed maps, rotated around the Galactic axis by multiples of  $10^\circ$  and/or flipped vertically and/or horizontally.

For a  $20^\circ$  Galactic cut, the correct template map has the highest of all 144 correlations, while the distribution of these correlations has standard deviation  $\Delta\hat{\alpha}_T \sim 2.5$  times larger than the formal errors  $\Delta\hat{\alpha}$ . Likewise, the correct DIRBE maps have the highest of all 144 correlations, and the standard deviations are  $\Delta\hat{\alpha}_T \sim \Delta\hat{\alpha}_M$ , even for a  $30^\circ$  Galactic cut (see Table 1). In contrast, we find no significant correlation between the 100  $\mu\text{m}$  and Haslam maps, indicating that synchrotron and dust emission are not strongly correlated at high latitudes.

Since both  $\Delta\hat{\alpha}_M$  and  $\Delta\hat{\alpha}_T$  have correlated signals contributing to the noise, they constitute overestimates of the true error bars.

### 3.2. Latitude Dependence

To investigate the dependence of the correlation on Galactic latitude, we sliced the maps into six regions of equal area, each corresponding to a range of latitude  $|b|$ . Figure 2 shows the results for the 100  $\mu\text{m}$  map. Note that  $\hat{\alpha}$  from the 19 GHz DIRBE correlation stays almost the same at each latitude band, indicating that this correlation is not dominated by one or two nearby clouds. The 19 GHz Haslam correlation is found to be more concentrated in the Galactic plane.<sup>6</sup>

<sup>6</sup> In order to test how important spatially localized features are for the correlation, we cross-correlated 19 GHz with Haslam using only one hemisphere. Most of the correlation was found to come from the northern hemisphere, presumably because of emission features such as the North Polar Spur.

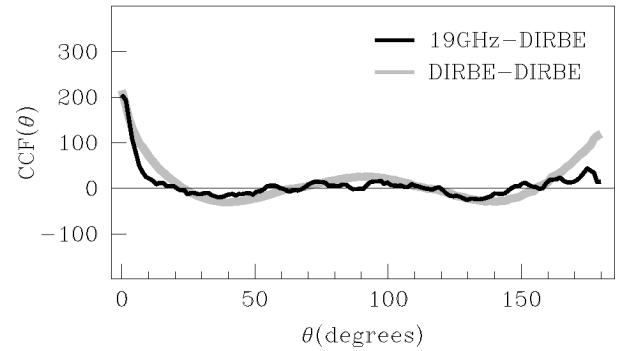


FIG. 3.—CCF( $\theta$ ) between 19 GHz and 140  $\mu\text{m}$  map for a  $30^\circ$  Galactic cut, together with the 140  $\mu\text{m}$  autocorrelation.

### 3.3. Scale Dependence

One way to determine angular scale of the correlation is to compute the angular cross-correlation function (CCF) of the 19 GHz map with the template maps. We computed this according to  $\text{CCF}(\theta) = [\sum_{ij} x_{\text{Gal},j} y_i / \sigma_i^2] / [\sum_{ij} \sigma_i^{-2}]$ , where the sums are again over all pairs of pixels separated by  $\theta$ .

As an example, Figure 3 shows the CCF( $\theta$ ) of the 19 GHz and 140  $\mu\text{m}$  maps as well as the autocorrelation function of the 140  $\mu\text{m}$  map. It is clear that the correlated structure in the two maps is on small angular scales ( $\theta \lesssim 10^\circ$ ) and that the CCF is well-behaved on all angular scales. The latter gives us additional confirmation that there are no large, unknown systematics that compromise the analysis. Similar results are found for the other two DIRBE maps. The lower signal-to-noise ratio for the correlation of the two radio templates result in CCFs which are less demonstrative. Note that  $\text{CCF}(0) \propto \hat{\alpha}$ .

As another way to investigate the dependence of the correlation on the angular scale, we repeated the analysis after high-pass filtering the 19 GHz map using a partial sky multipole removal technique (see Tegmark & Bunn 1995). Only after removing spherical harmonic components with  $\ell \gtrsim 8$  does the correlation significantly decrease, which again indicates that large-scale Galactic structure is not the source of the correlation. Both types of filtering therefore indicate that the bulk of the correlations are caused by fluctuations on scales of several degrees, which is consistent with the shape of the CCF in Figure 3.

## 4. CONCLUSIONS

The two synchrotron templates are found to be marginally correlated with the 19 GHz map, while all three DIRBE far-infrared templates show a significant correlation. When a synchrotron and a DIRBE template are simultaneously fit to the 19 GHz map (via linear regression), the correlation coefficients do not change significantly from those listed in Table 1 and, in addition, the two fit parameters are essentially uncorrelated ( $|\rho| \lesssim 0.05$ ). We conclude that the correlations with DIRBE dust emission are independent of the correlations with synchrotron emission. The amplitude of the signal is much larger than expected for ordinary (vibrational) dust emission, as shown in Figure 4. Moreover, there is now good agreement between different experiments that this correlated component is brighter at lower frequencies.

So what physical component is this? Two contenders have been proposed. Kogut et al. (1996a; K96b) argue on physical grounds that free-free emission might be spatially correlated

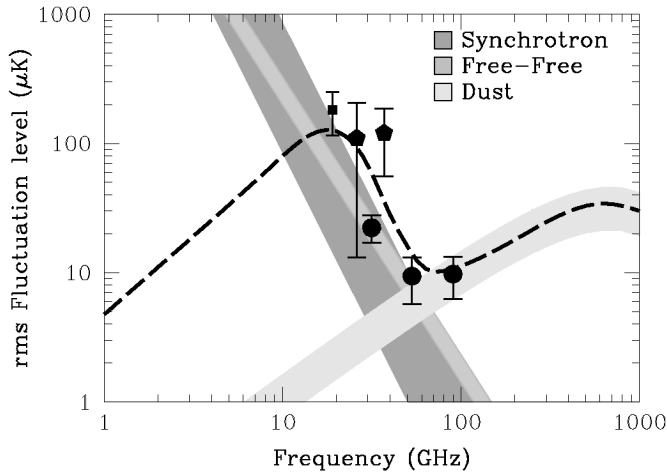


FIG. 4.—Frequency dependence of the fluctuating component of the Galactic emission for  $|b| > 30^\circ$ . The DMR correlations are represented by circles (K96b), Saskatoon data by pentagons (de Oliveira-Costa et al. 1997), and 19 GHz by a square with error bar given by  $\Delta\hat{\alpha}_r$  (this work). Dust emission (vibrational modes only) is normalized using the DMR correlation at 90 GHz (Kogut et al. 1996a). The free-free model is normalized to the DMR correlation at 31.5 GHz (the rms free-free emission derived from  $H\alpha$  is much smaller than this DIRBE-correlated component). The synchrotron emission is normalized to the correlation between the 19 GHz map and the 408 MHz Haslam map (see Table 1) and is consistent with the 31.5 GHz upper limits from K96b. The thickness of each curve corresponds to the normalization uncertainty. The dashed line is an example of emission from rotating dust grains (Draine & Lazarian 1998). All fluctuations have been converted to DMR angular scales as  $\delta T = \varepsilon \hat{\alpha} \sigma_{\text{Gal}}^i$ , where  $\sigma_{\text{Gal}}^i$  is the rms of each template map and the correction factor is  $\varepsilon = (\sum (2\ell + 1) \ell^\beta W_\ell^{\text{DMR}}) / (\sum (2\ell + 1) \ell^\beta W_\ell^i)^{1/2}$ . Here  $W_\ell^{\text{DMR}}$  is DMR window function,  $W_\ell^i$  is the window function of the experiment to be converted, and we assume a  $\beta = -3$  power spectrum slope.

with dust. However, the correlations between  $H\alpha$  (which is normally a good tracer of free-free emission) and CMB maps, and between  $H\alpha$  and the DIRBE maps, are weak (L97; Kogut 1997; McCullough 1997). One possibility is the presence of an extremely hot ( $\geq 10^6$  K), ionized plasma (L97); however, Draine & Lazarian (1998) have argued that this cannot be true across the whole sky on energetic grounds. These results motivated Draine & Lazarian to suggest that perhaps it is dust after all but emitting through rotational rather than vibrational excitations. As shown in Figure 4, this can give a spectrum quite similar to that of free-free emission in the relevant frequency range.

$H\alpha$  maps with better accuracy are currently being made by the Dennison, Gaustad, and Reynolds groups and should help to settle the issue. Another test is indicated by Figure 4: although both the rotating dust and the free-free models appear consistent with the available data,<sup>7</sup> the former predicts a bump and a downturn around 10–20 GHz, while the latter predicts a continued rise toward lower frequencies. A cross-correlation analysis with lower frequency data like the 10 GHz Tenerife map may be able to discriminate between these two models.

We would like to thank Ed Cheng, Dave Cottingham, Bruce Draine, Dale Fixsen, Ken Ganga, Ed Groth, Al Kogut, Alex Lazarian, George Smoot, and David Wilkinson for helpful comments. Support for this work was provided by NASA grants NAG5-6034 and NAG5-3015, by NSF grant PHY-9600015, by a David and Lucile Packard Foundation Fellowship (to L. P.), and by NASA through Hubble Fellowship HF-01084.01-96A from STScI, operated by AURA, Inc. under NASA contract NAS5-26555.

<sup>7</sup> We compute the spectral index between 19 and DMR 53 GHz to be  $\sim -2.4$  and that between 19 GHz and 1420 MHz to be  $\sim -2.8$ .

#### REFERENCES

- Bennett, C. L., et al. 1992, *ApJ*, 396, L7  
 Boggess, N. W., et al. 1992, *ApJ*, 397, 420  
 Boughn, S. P., et al. 1992, *ApJ*, 391, L49  
 Brandt, W. N., et al. 1994, *ApJ*, 424, 1  
 Cottingham, D. A. 1987, Ph.D. thesis, Princeton Univ.  
 de Oliveira-Costa, A., et al. 1997, *ApJ*, 482, L17  
 Draine, B. T., & Lazarian, A. 1998, *ApJ*, 494, L19  
 Gaustad, J. E., et al. 1996, *PASP*, 108, 351  
 Haslam, C. G. T., et al. 1981, *A&A*, 100, 209  
 Kogut, A. 1997, *AJ*, 114, 1127  
 Kogut, A., et al. 1996a, *ApJ*, 460, 1  
 ———. 1996b, *ApJ*, 464, L5 (K96b)  
 Leitch, E. M., et al. 1997, *ApJ*, 486, L23 (L97)  
 McCullough, P. R. 1997, *AJ*, 113, 2186  
 Reich, P., & Reich, W. 1988, *A&AS*, 74, 7  
 Simonetti, J. H., et al. 1996, *ApJ*, 458, L1  
 Tegmark, M., & Bunn, E. 1995, *ApJ*, 455, 1  
 Tegmark, M., & Efstathiou, G. 1996, *MNRAS*, 281, 1297  
 Weiss, R. 1980, *ARA&A*, 18, 489